Journal of The Electrochemical Society

OPEN ACCESS

Revealing the Local pH Value Changes of Acidic Aqueous Zinc Ion Batteries with a Manganese Dioxide Electrode during Cycling

To cite this article: Christian Friedrich Bischoff *et al* 2020 *J. Electrochem. Soc.* **167** 020545

Journal of The Electrochemical Society, 2020 **167** 020545

Revealing the Local pH Value Changes of Acidic Aqueous Zinc Ion Batteries with a Manganese Dioxide Electrode during Cycling

Christian Friedrich Bischoff,[1,z] Oliver Sebastian Fitz,[1] Jordan Burns,[2] Manuel Bauer,[1] Harald Gentischer,[1] Kai Peter Birke,[3] Hans-Martin Henning,[4] and Daniel Biro[1]

[1]*Battery Cell Technology, Department of Electrical Energy Storage, Fraunhofer Institute for Solar Energy Systems ISE, Freiburg, Germany*
[2]*Applied Energy Materials Group, Energy Storage & Distributed Resources Division, Energy Technologies Area, Lawrence Berkeley National Laboratory, Berkeley, California, United States of America*
[3]*Chair for Electrical Energy Storage Systems, Institute for Photovoltaics (*ipv*), University of Stuttgart, Stuttgart, Germany*
[4]*Chair of Solar Energy Systems, Institute for Sustainable Technical Systems (INATECH), University of Freiburg, Freiburg, Germany*

The research on aqueous zinc ion batteries (AZIB) is getting more attention as the energy transition continues to develop and the need for inexpensive and safe stationary storage batteries is growing. As the detailed reaction mechanisms are not conclusively revealed, we want to take an alternative approach to investigate the importance of pH value changes during cycling. By adding a pH-indicator to the electrolyte (2 M $ZnSO_4$ + 0.1 M $MnSO_4$), the local pH-value change during operation is visualized in operando. The overall pH value was found to increase during cycling whereas a major temporary pH drop in close proximity of the manganese dioxide electrode surface occurs. Additionally, this pH value change was quantified locally by in operando measurements with a pH micro electrode. Different electrolyte compositions with additives (sodium dodecyl sulfate (SDS), sulfuric acid (H_2SO_4)) and operation voltages were tested. The pH-potential-diagrams of manganese and zinc reveal pH value and potential limits, leading to active material dissolution at lower pH values and oxygen gas evolution at higher potentials >1.7 V. The procedure of combining a pH indicator, pH microelectrode measurements and pH-potential diagrams can be seen as an appropriate method to determine the recommendable working window of aqueous batteries.
 [DOI: 10.1149/1945-7111/ab6c57]

Manuscript submitted October 28, 2019; revised manuscript received December 28, 2019. Published January 30, 2020.

Supplementary material for this article is available online

As a consequence of the expansion of renewable energy systems, the need for efficient energy storage systems is intensifying. Electrochemical energy storage technologies like batteries are able to save energy during the course of a day efficiently making them interesting for home storage and network balancing applications. The market for stationary battery systems is expanding with lower demands concerning the gravimetric and volumetric energy density compared to mobile battery systems. This different requirement profile makes alternative and environmentally-friendly cell chemistries, which would be too bulky for mobile applications, possible for stationary storage applications. One of the promising alternative battery technologies is the so called zinc ion battery (ZIB) with acidic aqueous electrolyte. ZIBs use zinc as the negative electrode material, mainly manganese dioxide as the positive electrode material and an aqueous zinc salt solution as electrolyte.[1] The raw materials such as zinc and manganese oxides are abundant globally[2] and are environmentally friendly. Nevertheless, there are still issues in terms of the reaction mechanism of the ZIB cell chemistry. The full understanding of the reaction mechanism is important for the production parameters like the electrode thickness and its porosity as well as the electrolyte composition.

Until now, and to the best of our knowledge, the following reaction mechanisms have been discussed in literature so far:

- Zn^{2+}-intercalation/-extraction[3–7]
- H^+ intercalation/-extraction and conversion reaction of a zinc hydroxide sulfate species (ZHS)[8–10]
- H^+ and Zn^{2+} co-intercalation in different charge and discharge steps[11–13]
- combination of H^+ and Zn^{2+} co-intercalation and conversion reaction[14]

For the examination of the reaction mechanisms, in most of the relevant publications ex situ investigation methods such as X-ray diffraction (XRD),[3,5,6,8–22] X-ray photoelectron spectroscopy (XPS)[10,13,17–22] (for investigating the crystalline structure of the manganese dioxide active material at different cycling steps), transmission electron microscope (TEM) (and High-resolution transmission electron microscope (HR TEM)),[5,6,9,10,13,22] scanning electron microscope (SEM)[5,9,10,13,14,17,19] (both for investigating the surface changes of the manganese dioxide electrode at different cycling steps) and X-ray absorption spectroscopy (XAS)[3,4,6] were used. To carry out these methods, cycled batteries had to be disassembled and electrodes had to be rinsed with DI-water. A few publications used in situ methods like in situ XRD[5,8,20] and X-ray absorption near-edge structure (XANES).[5]

Moreover, the overall importance of the pH value in ZIBs during cycling seems to play a major role in terms of the understanding of the reaction mechanisms taking place during charging and discharging of ZIBs. In Lee et al. (2016),[8] the pH value changes were logged in operando during cycling in a PTFE Swagelok© union tee by a pH meter. This way only the overall pH value changes of the bulk electrolyte could be measured. The measurements showed a pH lift from start of discharge with a pH value of 4.62 to 5.73 after discharge.[8] In Chamoun et al. (2018),[23] the same experimental set up was used and the pH values of the bulk electrolyte were measured every 5 min. In this particular investigation the overall pH value reaches a value of 5.22 (Mn^{2+} free electrolyte) and 4.76 (added Mn^{2+}), respectively. These results will be taken into account later. In general, manganese sulfate (mostly with the concentration of 0.1 M) is used as an additive in the zinc sulfate electrolyte of zinc ion batteries to lessen the manganese dissolution of the positive electrode during cycling.[9,23] Besides the reaction mechanism and the pH value change, the manganese dioxide dissolution and degradation remains an issue in the current literature.[6,23,24] Some recent investigations take advantage of the manganese dissolution/deposition and use it intentionally as a reaction mechanism in the

[z]E-mail: Christian.Bischoff@ise.fraunhofer.de

positive electrode.[13,25] Others enhance the rechargeability of the cell by doping the active material of the positive electrode,[26] by focusing on the negative zinc electrode[27] or by introducing alternative electrolytes.[28–30]

In this investigation we try to take a further step towards the understanding of the reaction mechanism and operating parameters by means of an in operando investigation method using a pH indicator (added to the electrolyte) to visualize, and a thin pH micro electrode to quantify, the local pH changes in the electrolyte during cycling (Section: "Cell cycling: local pH value changes at positive/negative electrode"). Experimental cells with different electrolyte compositions were tested in cyclic voltammetry measurements in advance to prove the absence of influence of the chosen pH indicator in the electrolyte on the electrochemical performance (Section: "CV measurements: chemical stability of pH indicators in electrolyte solution").

A closer look on a potential-pH-diagram (Pourbaix diagram) shows the thermodynamic thresholds of the electrochemical system and when the manganese dissolution possibly starts is also dependent on the pH value and the potential. An operational window can be defined for the ZIB system using zinc and manganese dioxide as active materials and aqueous zinc sulfate with manganese sulfate electrolytes by sketching the reaction path into the diagram (Section: "Pourbaix diagram: thermodynamic working window of ZIBs"). Based on these results, two different electrolyte additives are tested and the operational window of the battery is changed in order to achieve a better understanding of the occurring phenomena.

Experimental

Materials.—For the positive electrode preparation, 70 wt% manganese dioxide (Manganese(IV) oxide, 99.9 % (metals basis), 325 mesh powder, Alfa Aesar, for XRD measurements (Supplementary S1, available online at stacks.iop.org/JES/167/020545/mmedia), 20 wt% Carbon black (Carbon black, acetylene, 100 % compressed, 99.9 + %, Alfa Aesar) and 10 % binder (LA 133, GELON LIB group) were mixed with a speedmixer (DAC 150.1 FVZ-K, Hauschild & Co.KG, Germany) with 3000 rpm for 90 s. Subsequently, the positive electrode slurry was homogenized in a three-roll mill (EXAKT 80E) with a final roll gap of 5 μm to control and unify the particle sizes. A stainless steel foil (1.4301/AISI 304, thickness 25 μm, TBJ Industrieteile GmbH, Germany) was coated with a doctor blade (mass loading 0.6–1.4 mg cm^{-2}). As negative electrode, a 25 μm thick zinc foil was used with a purity of 99.95 %.

As pH indicator, bromocresol green was chosen because its color change point from yellow (low pH values) to blue (high pH values) is located between pH 3.8 and 5.5.[31] This pH range includes the initial pH value of the standard electrolyte. Therefore, pH value changes of the standard electrolyte can be visualized.

Four types of electrolytes were mixed and used for the investigation of the pH value changes:

a) standard electrolyte: 2 M $ZnSO_4$ + 0.1 M $MnSO_4$, pH 4.3,
b) standard electrolyte with 0.66 % (w/w) pH indicator bromocresol green (1 % (w/w) in ethanol, Alfa Aesar) as additive,
c) standard electrolyte with 1 CMC (critical micelle concentration) sodium dodecyl sulfate (SDS), pH 4.4,
d) standard electrolyte with 0.27 % (w/w) of 20 % sulfuric acid, pH 1.9.

Electrolyte c) and d) were exclusively used in Section "Pourbaix diagram: thermodynamic working window of ZIBs".

Cell assembly.—Experimental cells were assembled using cuvettes usually used for UV-vis spectroscopy measurements (polystyrol, 10 × 10 × 45 mm) in order to achieve a good visibility of any color changes occurring while cycling. Positive and negative electrode sheets (coated area 9 × 25 mm) were attached to each side of the cuvette and each electrolyte composition was filled into the cuvette cell until the positive electrode coating was covered by the electrolyte solution (Fig. 1).

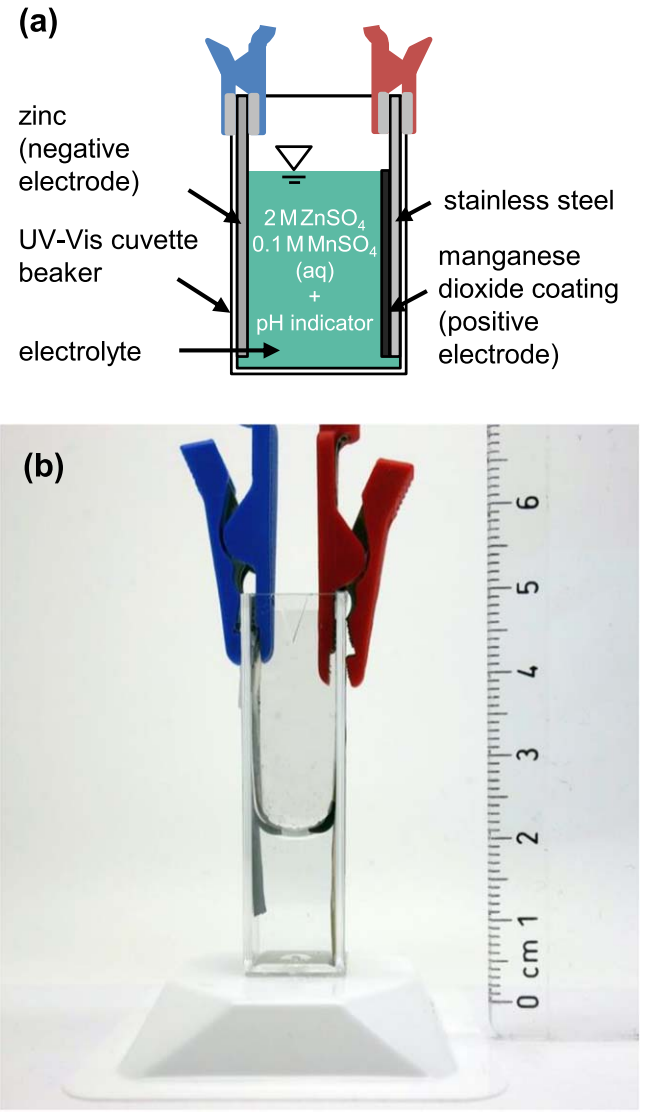

Figure 1. Schematic drawing of the utilized cuvette test cell (a); photo of the cuvette cells (b) with the zinc electrode on the left, manganese dioxide electrode on the right (without pH indicator for a better view).

Characterization methods.—The cyclic voltammetry measurements were performed with 0.1 mV s^{-1} between 0.9 to 1.9 V by using a BioLogic VMP3 potentiostat.

The cell cycling was performed with 40 mA g^{-1} (related to active material loading of the manganese dioxide electrode) from 0.9 to 1.9 V with a BioLogic VMP3 potentiostat.

To verify the visual pH measurements with the pH indicator, a pH micro electrode (ORION 9863BN with METTLER TOLEDO SevenMulti S47) with a glass tip diameter of 1.7 mm was used to determine the pH values at several states of charge and discharge at three different positions (Fig. 5).

Results and Discussion

CV measurements: chemical stability of pH indicators in electrolyte solution.—In order to investigate the chemical stability of the pH indicator used as an additive in the standard electrolyte, cyclic voltammetry measurements (CV) between 0.9 and 1.9 V were conducted on full cells. The results are shown in Fig. 2.

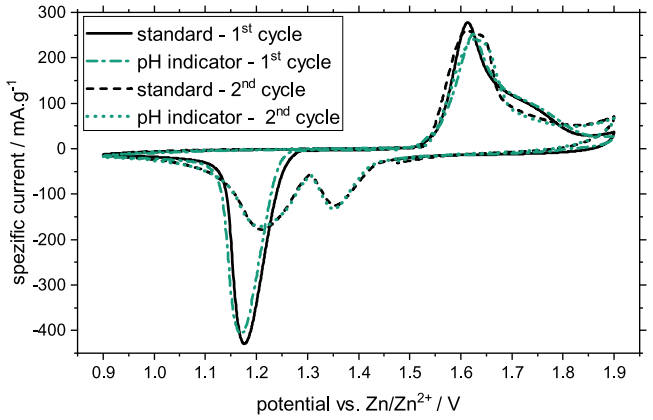

Figure 2. The first two cycles of the cyclovoltammetry measurements (0.1 mV s^{-1}) conducted on full cells with the standard electrolyte vs the electrolyte with the addition of bromocresol green.

The CV curve of the cell with the bromocresol green shows no significant differences in the anodic and cathodic reactions compared to the one with the standard electrolyte. This result enables the assumption that no side reactions were induced by the addition of bromocresol green. So the bromocresol green should have no major influence on the redox reactions of the zinc ion battery cell and can be used to indicate the pH value changes during cycling.

Cell cycling: local pH value changes at positive/negative electrode.—In order to localize and visualize the pH-value changes during cycling, a time-lapse photo of the battery was taken every 60 s (Fig. 3, for more photos see Supplementary S2). The cell was initially discharged to 0.9 V and subsequently charged/discharged to 0.9/1.9 V once by applying a current density of 40 mA g^{-1} (related to the mass of active material). Afterwards, the photos taken during cycling were assigned to the cell potential, respectively, to visualize the color changes of the pH indicator in relation to the cell potential and the reaction taking place.

In the beginning, the electrolyte is greenish colored (Fig. 3a). This indicates that the pH value is about 4.3, which was confirmed by pH measurements (Fig. 6). When the cycling process was started, the electrolyte color changed from greenish to deep blue (Figs. 3b–3c), which indicates a pH value increase.

During the initial discharge and the first charge step, the color of the electrolyte remains blue (Fig. 3c). In Fig. 3d, a local yellow colouration of the electrolyte in front of the manganese dioxide electrode is occurring, starting at about 1.7 V and indicating a strong pH value decrease.

The potential mapping of the different photos taken of the zinc ion battery cell with bromocresol green is shown in Fig. 4. The corresponding points to Fig. 3 are marked in the diagram with alphabetic letters (Fig. 4). The specific discharge capacity of this cell was 110.0 mAh g^{-1} (related to the active material mass loading). A symmetric Zn/Zn cell with the same electrolyte and in the same test cell configuration was cycled to study the polarization behavior of the negative zinc electrode and the cell configuration (Supplementary S3). The overpotential of this cell was found to be about ±30 mV. Therefore the negative metallic zinc electrode can be considered as a quasi-reference electrode which leads to a maximum potential shift of <5 % between the measured cell potential and the positive electrode potential.

Obviously, the yellow coloring of the colored electrolyte occurs at higher potentials above 1.7 V vs Zn/Zn^{2+} and indicates either the formation of H_3O^+-ions or the consumption of OH^--ions in front of the manganese dioxide electrode at higher cell potentials.

During the cycling of the cell, a slight decolorization of the electrolyte could be noticed, which could be attributed to the zinc electrode by performing OCV experiments with a cell only containing a zinc electrode with standard electrolyte including pH indicator (Supplementary S4). Considering the CV comparison in Fig. 2, where no major influence of the pH indicator on the electrochemical performance of the cell could be detected, the observation of decolorization should not be notably affecting the positive electrode reaction and the cycling performance of the cell (Section: "CV measurements: chemical stability of pH indicators in electrolyte solution").

In order to quantify and verify the local pH value changes during cycling, a pH micro electrode was inserted to measure the pH values in operando at different places. The current pH value was measured every two minutes in different spatial arrangements (Fig. 5).

The results shown in Fig. 6 affirm the pH drop at higher potentials during charging indicated by the bromocresol green in Figs. 3d–3f. This pH value drop is only taking place in front of the manganese dioxide electrode.

The pH value drop and the local yellow colouration of the pH indicator can be explained by the oxygen evolution reaction (OER)[32]:

$$6H_2O \rightleftharpoons O_2 + 4H_3O^+ + 4e^- \quad (E_0 = +1.23V \text{ vs SHE}) \qquad [1]$$

The electrons are removed from the manganese dioxide electrode (working as the anode) during the charge step and therefore the reaction equilibrium is pulled to the right side (Eq. 1). As a result,

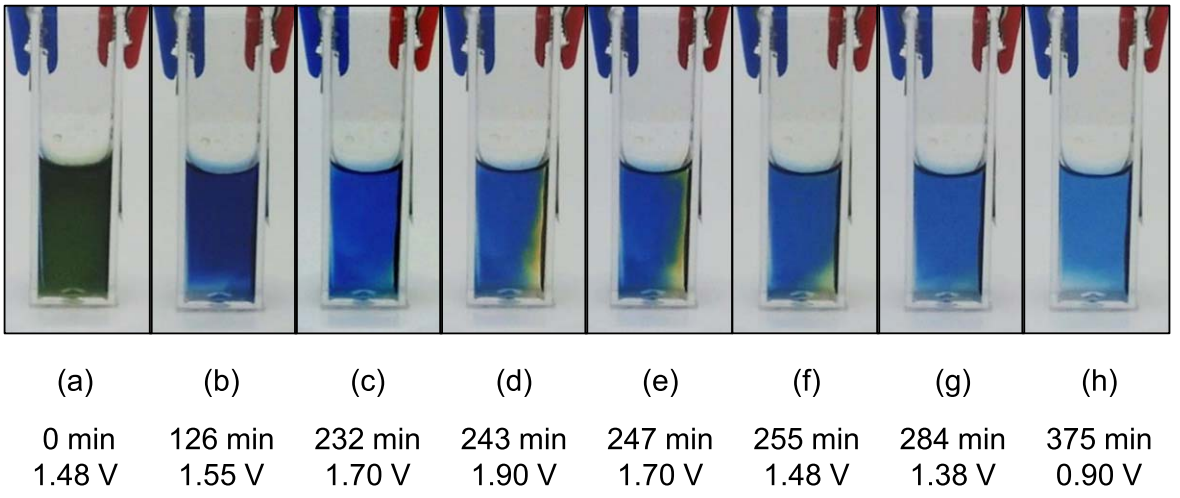

Figure 3. Photos of the zinc ion battery cell in UV-vis cuvette casing at different states of charge together with the cell potential and the resulting color of the pH indicator additive in the electrolyte. Blue clamp (left): negative zinc electrode, red clamp (right): positive manganese dioxide electrode.

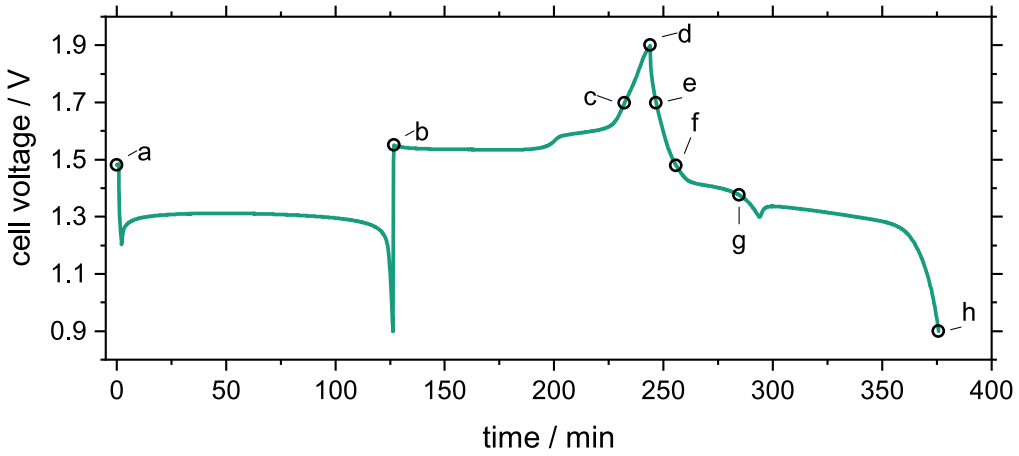

Figure 4. Potential curve of the zinc ion battery shown in Fig. 3 with markers at every state of charge were a photo image was taken.

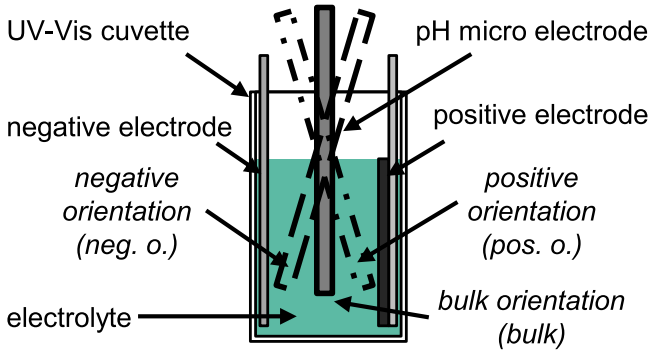

Figure 5. Schematic presentation of the spatial arrangement of the pH electrode for the in operando pH value measurements. Right: manganese dioxide electrode. Left: zinc negative electrode. Middle: pH micro electrode with different orientations.

the surrounding electrolyte becomes increasingly acidic because of the formation of H_3O^+ ions and shifts the color of the added bromocresol from green to yellow.

The steady rise of the pH value during the initial discharge might be linked to the dissolution of manganese dioxide (thermodynamically possible in this pH-potential area, Fig. 7), which is also described in:[8,23,32]

$$MnO_2 + 2H_2O + 2e^- \rightleftharpoons Mn^{2+} + 4OH^- (E_0 = +1.23V \text{ vs SHE}) \quad [2]$$

Moreover, the steady rise of the pH value during the initial discharge and the following discharge steps can be described with the insertion of H^+ ions:[6,11,19,33]

$$MnO_2 + H_2O + e^- \rightleftharpoons MnOOH + OH^- \quad (E_0 = +0.19V \text{ vs SHE for } \beta\text{-}MnO_2) \quad [3]$$

The formed hydroxide ions (Eqs. 2 and 3) lead to an increase of the pH value of the electrolyte during discharge. The initial mildly acidic electrolyte (pH 4.3, occurring green when the electrolyte is colored with bromocresol green) becomes more neutral during cycling. This triggers the precipitation of zinc hydroxide sulfate.[8] The evolution of zinc hydroxide sulfate consumes hydroxide ions (Eq. 4) and therefore buffers the pH value:

$$4Zn^{2+} + SO_4{}^{2-} + 6OH^- + 5H_2O \rightleftharpoons Zn_4SO_4(OH)_6 \cdot 5H_2O \quad [4]$$

During the further reaction mechanism steps, more hydroxide is evolved which is buffered by zinc hydroxide sulfate and therefore avoids any higher pH value increase.[23] The standard potentials of the zinc hydroxide sulfate half reactions are difficult to specify because these reactions occur in a broader potential window during the redox reaction processes in aqueous zinc ion batteries.[14]

From the start of the pH value drop in Fig. 6 (marker (c) in Fig. 4) until the relaxation to its original value (marker (g) in Fig. 4), it takes about 52 min in total. For about 15 min, the manganese dioxide electrode is exposed to the potential >1.7 V, where the OER reaction takes place (between marker (c) and (e) in Fig. 4). The pH drop caused by the OER is buffered back to the stabilized pH value of ~5.1 in a time range of about 37 min (between marker (e) and (g) in Fig. 4).

This phenomenon might either indicate the insertion of the H^+ ions during the discharge process or the recombination of H^+ ions with the OH^- resulting from Eq. 3. Both options are simultaneously possible.

The mean pH values shown in Fig. 6 are slightly higher than the logged pH value of 4.78 shown in Chamoun et al. (2018)[23] and 4.64 in Lee et al. (2016).[8] This can be explained by the much higher volume of electrolyte in the UV-vis cuvette battery cell as the pH value represents the concentration of H_3O^+ ions per volume unit. Furthermore, the active mass loading of the electrodes is comparatively high in Chamoun et al. (2018)[23] and Lee et al. (2016),[8] which brings a higher charge and ion transfer, respectively. As seen in Chamoun et al. (2018), the pH value in Fig. 6 reaches a stable plateau because of the buffering effect of the zinc hydroxide sulfate formation (Eq. 4).

Pourbaix diagram: thermodynamic working window of ZIBs.— With the help of the results shown above, the thermodynamic working window of the zinc ion battery can be sketched in a pH-potential diagram, also known as Pourbaix diagram. In order to visualize the relevant potential-pH area for the zinc ion battery, the Pourbaix diagram of manganese and zinc were overlaid in a single diagram. The ion concentrations of manganese and zinc were chosen as 0.1 M and 2.0 M, respectively, under consideration of the electrolyte concentrations. The upper frame defines the thermodynamic working window of the positive electrode, here the manganese dioxide electrode, and the lower frame outlines the thermodynamic working window (considering overpotentials for the zinc plating/stripping due to nucleation phenomena,[34,35]) of the negative electrode, here the zinc electrode. The potentials are referenced to the standard hydrogen electrode (SHE) as well as to the zinc electrode (Zn/Zn^{2+}). The dashed lines show the hydrogen (lower line) and oxygen (upper line) gas evolution.

Obviously, the manganese dissolution, which was already described in preceding studies,[9] is strongly dependent on the pH value and the electrical potential.

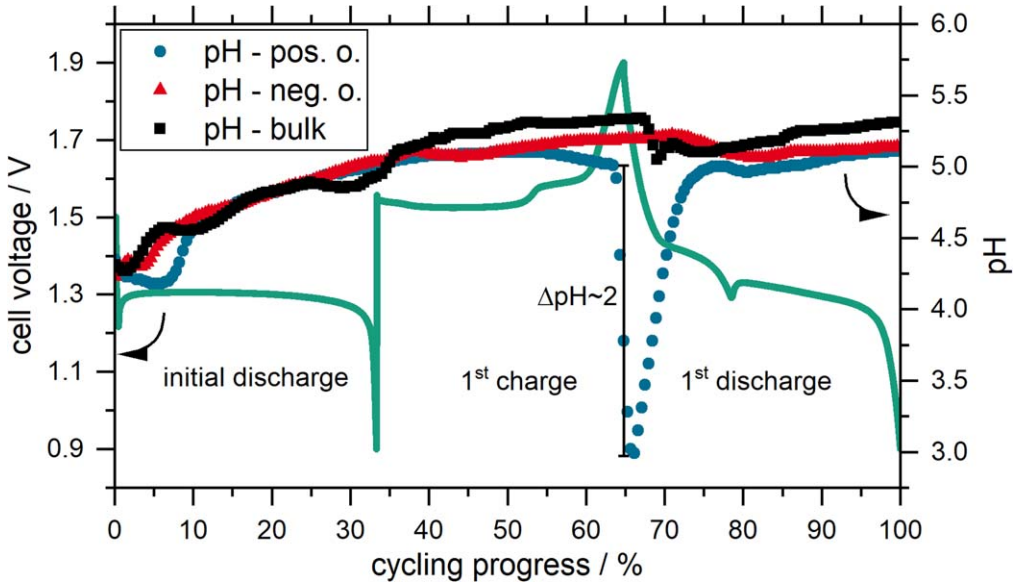

Figure 6. Potential curve of the zinc ion battery full cell during initial discharge and first cycle together with the corresponding pH value at the different spatial arrangements of the pH micro electrode. A relative pH value drop of about 2 was detected.

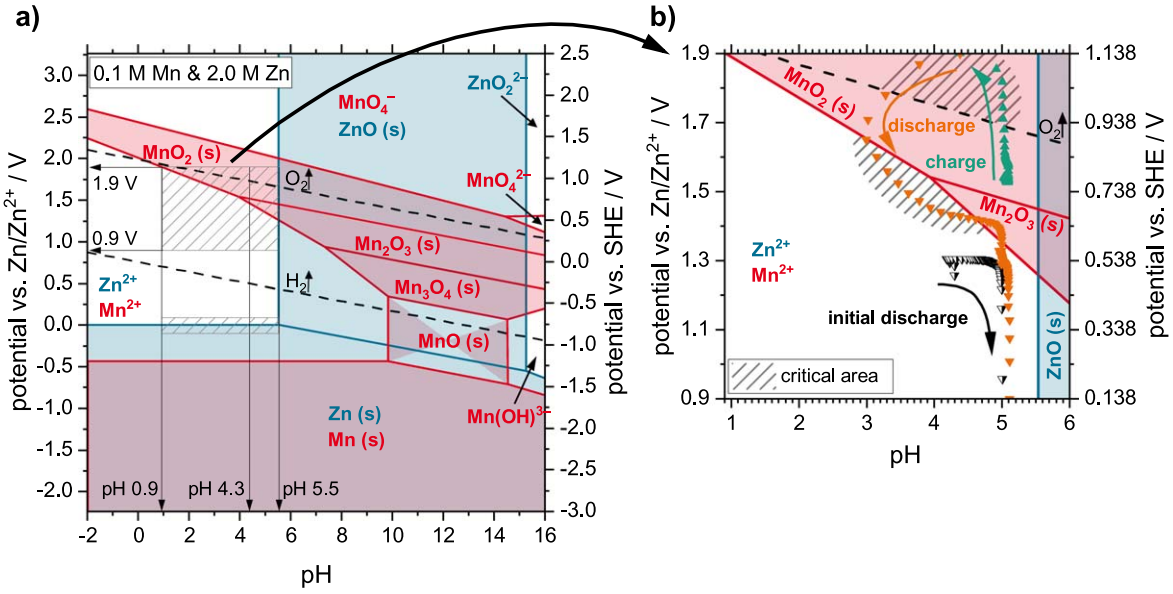

Figure 7. (a) Thermodynamic working window of zinc ion battery chemistry regarding the pH value. Overlay of Pourbaix diagrams (kindly provided by Materials Project of the University of California at Berkeley, www.materialsproject.org,[50]); (b) zoom and pH-potential plot of the cell cycling path of the battery cell with the standard electrolyte composition shown in Fig. 6 (positive orientation, shaded area should be avoided for longer duration). For more details about this diagram see the following section.

In the literature concerning zinc ion batteries, the batteries are commonly cycled in a potential window between 1.9 V and 0.9 V vs Zn/Zn^{2+} which is equivalent to 1.14 V and 0.14 V vs SHE (Fig. 7). For the redox reaction of the zinc electrode

$$Zn^{2+} + 2e^- \rightleftharpoons Zn \quad (E_0 = -0.76V \text{ vs SHE}) \qquad [5]$$

−0.76 V vs SHE is needed which is possible up to a pH value of 5.6.[32] Higher pH-values foster the generation of zinc oxide precipitation on the surface of the electrode.

In summary, the overlay of the Pourbaix diagrams of zinc and manganese shows a well-defined thermodynamic working window and a high relevance of the pH value for the rechargeability of a zinc ion battery. Low pH values are desirable in order to prevent the precipitation of zinc oxide on the negative electrode but they also foster the dissolution of manganese dioxide, which can partly be prevented by the addition of manganese sulfate in the electrolyte.[9]

The Pourbaix diagram shows the possibility of an oxygen evolution reaction (OER) inside the working window of the manganese dioxide electrode defined above. Regarding the pH values of slightly over 5 in Fig. 6 during cycling, we can identify a potential of ∼1.7 V vs Zn/Zn^{2+} as the critical potential for the starting of the OER. The manganese dioxide electrode is exposed to this pH-potential-area for the duration of about 15 min during the measurement in Fig. 4, which leads to the OER (Eq. 1) and to the decrease of the pH value.

To reduce the OER, there are two possible solutions considering the Pourbaix diagram:

- reduction of the pH value to increase the necessary potential for the OER
- reduction of the end-of-charge voltage to ∼1.7 V vs Zn/Zn^{2+} to prevent the cell potential of crossing the OER potential

Furthermore, another possible solution is to widen the stability window of the aqueous electrolyte through the addition of additives. Hou et al. (2017)[36] could expand the operation window of their aqueous electrolyte (1 M Na_2SO_4 with 1 M $ZnSO_4$) to about 2.5 V by the addition of SDS: The SDS molecules are adsorbed electrostatically on the surface of the electrodes and therefore build up a hydrophobic layer.[36] This hydrophobic layer is supposed to suppress the hydrogen or oxygen evolution by preventing the contact between the water molecules and the electrodes.[36]

Figure 8 shows the resulting pH value behavior of the three adjusted electrolytes (c) and (d) (Section: "Materials") and end-of-charge-voltages, respectively, in front of the manganese dioxide electrode (positive electrode orientation).

The addition of 1 CMC SDS (Fig. 8a) with its corresponding cell cycling path in the pH-potential diagram (Fig. 8b) could not show any significant influence on the OER at higher potentials and the resulting pH value drop, compared to the standard electrolyte composition shown in Fig. 7b.

The reduction of the pH value by the addition of sulfuric acid (Fig. 8c) with its corresponding cell cycling path in the pH-potential diagram (Fig. 8d) showed three significant changes in the cycling behavior:

- the starting potential of the OER is increased from ~1.5 V to ~1.7 V,
- the size of the relative pH drop is decreased from $\Delta pH \approx 2$ (Fig. 6) to $\Delta pH \approx 1.1$ (Fig. 8c),
- the pH value steadily increases while cycling the cell.

The manganese dissolution and the formation of OH^--ions becomes obvious when looking at Fig. 8 (d), because most of the cell cycling path is located in the critical area of manganese dissolution. Thus, the formation of OH^--ions (Eq. 2) is fostered, resulting in a steady pH value increase.

For fully understanding the effects and influences of both the reduction of the pH value by the addition of sulfuric acid, as well as the addition of a surfactant like SDS, further investigation is necessary.

The limitation of the end-of-charge voltage from 1.9 to 1.7 V (Fig. 8e) shows no significant pH value drop anymore. Furthermore, this fact gets obvious when looking at the corresponding cell cycling path in Fig. 8f: After the initial discharge step, while charging/discharging the cell, the pH-potential path is a nearly vertical line, showing no significant pH value change.

This fact shows the adaptability of the Pourbaix diagram and the theory of an OER at higher potentials >1.7 V. The limitation of the

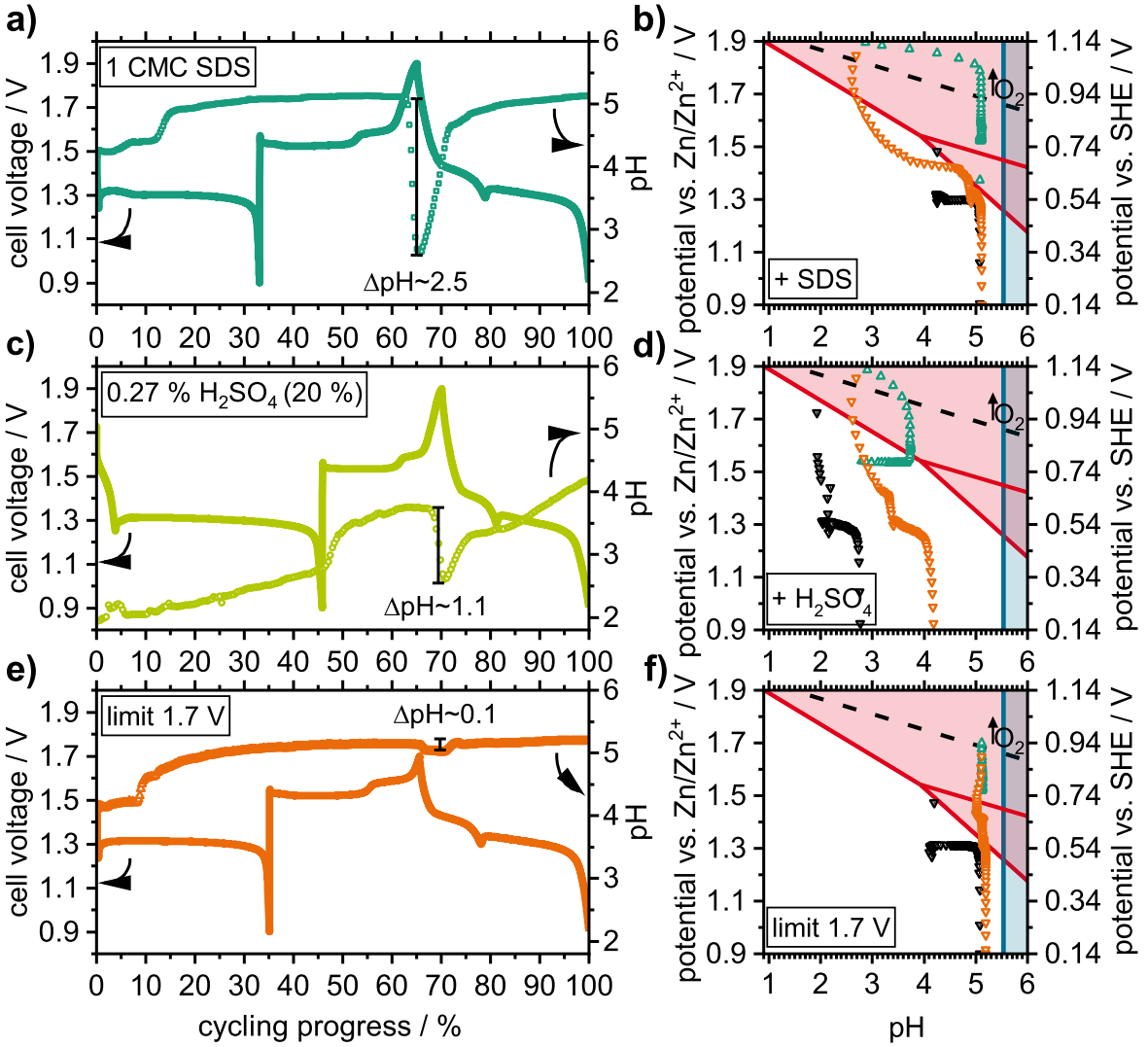

Figure 8. Potential curve in combination with the pH value curve with positive electrode orientation of the three different cell setups with the addition of 1 CMC SDS (a), the addition of 0.27 % of 20 % sulfuric acid (c) and the limitation of the end-of-charge voltage to 1.7 V (e). On the right side, the corresponding pH-potential diagrams with the cell cycling path of each electrolyte composition (addition of SDS (b), addition of sulfuric acid (d) and the limitation to 1.7 V (f)) is shown.

end-of-charge voltage with its resulting cell cycling behavior can therefore be one possible solution to prevent the cell from the OER. This result was also confirmed by a visual test with bromocresol green as indicator (Supplementary S5), when no color change of the indicator became visible.

However, a limitation of the end-of-charge voltage results in a loss of energy storage capability. An illustrative calculation of the specific capacity and energy storage capability losses caused by the limitation of the end-of-charge voltage to 1.7 V showed a decrease in specific capacity of ∼9 %, leading to a decrease in specific energy of ∼12 %. Applying a constant voltage phase at ⩽1.7 V (CV phase) for the charging step could reduce the loss in specific energy to ∼1.5 % (Supplementary S6).

Regarding the cell architecture used in this work (UV/VIS cuvettes), it should be taken into account that the amount of the electrolyte is relatively high (∼2–3 ml) and the distance between the electrodes is high (∼9 mm) compared to button cells, for example. This fact can have further influences on the cycling performances of both the zinc and manganese dioxide electrode due to the local pH value changes.

Nevertheless, the OER seems to be an underestimated problem as the common voltage window in Zn//MnO2 batteries is normally in the range of 0.7–1.1 V as the end-of-discharge voltage and 1.7–2.0 V as the end-of-charge voltage, respectively (Supplementary S7).[3–23,37–48]

Constant voltage steps at a high voltage level, like in Chamoun et al. (2018),[23] should be especially avoided in commercialized battery systems. The end-of-discharge voltages are likely not critical compared to the end-of-charge voltages which foster oxygen evolution. Adding a pH buffer, as suggested in Huang et al. (2019),[49] might be reasonable and needs to be investigated in future work.

Conclusions

The local pH value changes during the initial discharge and the first cycling steps of a zinc/manganese dioxide battery with mildly acidic aqueous electrolyte were displayed. New methods of adding pH indicator to the electrolyte and by using UV-vis cuvettes as battery cells to display local color changes in operando were introduced. It was shown that the initial pH value of 4.3 of the electrolyte increases during cycling and stabilizes at a pH value of about 5.2 after the first cycle. In a potential-pH diagram of zinc and manganese it was shown that a pH value above 5.6 should be avoided because otherwise zinc oxide precipitation would passivate the zinc electrode. Higher zinc sulfate concentrations (above 2 M $ZnSO_4$) are recommended to remain in a lower pH value area. Furthermore, higher manganese sulfate concentrations in the electrolyte (above 0.1 M $MnSO_4$) could lower the manganese dioxide dissolution by shifting the chemical reaction equilibrium to the back reaction side.

High end-of-charge voltages (above 1.7 V vs Zn/Zn^{2+}) are causing strong local pH value drops at the end of charge/beginning of discharge because of the OER in front of the manganese dioxide electrode, which was shown by measurements with a pH micro electrode.

The pH value drop can be nearly avoided when the end-of-charge potential is lowered to 1.7 V, or reduced when the pH value of the electrolyte is lowered by adding sulfuric acid. Widening the stability window using additives could be another solution for the gas evolution problem. The pH changes might become even stronger when the amount of electrolyte and the distance between the electrodes are reduced for more industry-oriented cell architectures.

Appropriate measures to suppress gas evolution become important when this type of battery is commercialized: Thicker electrodes to achieve higher energy densities cause higher internal resistances resulting in higher overpotentials during cycling. Limiting the end-of-charge voltage to 1.7 V followed by a constant voltage phase as well as carefully chosen additives should be adequate solutions for this problem.

Consequently, in further investigations, the gas evolution and its accompanying species at the manganese dioxide electrode should be taken into account when the upper limit of the charge potential is accordingly high.

Acknowledgments

Christian Bischoff acknowledges the *Heinrich Böll Stiftung* and Oliver Fitz acknowledges the *Deutsche Bundesstiftung Umwelt* for the support.

References

1. V. Verma, S. Kumar, W. Manalastas, R. Satish, and M. Srinivasan, "Progress in rechargeable aqueous zinc- and aluminum-ion battery electrodes: challenges and outlook." *Adv. Sustain. Syst.*, **3**, 1800111 (2018).
2. *Mineral Commodity Summaries 2019*, U.S. Geological Survey (2019), https://usgs.gov/centers/nmic/mineral-commodity-summaries (accessed on 6 June 2019).
3. M. H. Alfaruqi, J. Gim, S. Kim, J. Song, J. Jo, S. Kim, V. Mathew, and J. Kim, "Enhanced reversible divalent zinc storage in a structurally stable α-MnO_2 nanorod electrode." *J. Power Sources*, **288**, 320 (2015).
4. M. H. Alfaruqi, S. Islam, J. Gim, J. Song, S. Kim, D. T. Pham, J. Jo, Z. Xiu, V. Mathew, and J. Kim, "A high surface area tunnel-type α-MnO_2 nanorod cathode by a simple solvent-free synthesis for rechargeable aqueous zinc-ion batteries." *Chem. Phys. Lett.*, **650**, 64 (2016).
5. M. H. Alfaruqi, V. Mathew, J. Gim, S. Kim, J. Song, J. P. Baboo, S. H. Choi, and J. Kim, "Electrochemically induced structural transformation in a γ-MnO_2 cathode of a high capacity zinc-ion battery system." *Chem. Mater.*, **27**, 3609 (2015).
6. N. Zhang, F. Cheng, J. Liu, L. Wang, X. Long, X. Liu, F. Li, and J. Chen, "Rechargeable aqueous zinc-manganese dioxide batteries with high energy and power densities." *Nat. Commun.*, **8**, 405 (2017).
7. C. Xu, S. W. Chiang, J. Ma, and F. Kang, "Investigation on zinc ion storage in alpha manganese dioxide for zinc ion battery by electrochemical impedance spectrum." *J. Electrochem. Soc.*, **160**, A93 (2012).
8. B. Lee, H. R. Seo, H. R. Lee, C. S. Yoon, J. H. Kim, K. Y. Chung, B. W. Cho, and S. H. Oh, "Critical role of pH evolution of electrolyte in the reaction mechanism for rechargeable zinc batteries." *Chem. Sus. Chem.*, **9**, 2948 (2016).
9. H. Pan et al., "Reversible aqueous zinc/manganese oxide energy storage from conversion reactions." *Nat. Energy*, **1**, 16039 (2016).
10. Q. Zhao et al., "Unravelling H^+/Zn^{2+} synergistic intercalation in a novel phase of manganese oxide for high-performance aqueous rechargeable battery." *Small*, e1904545 (2019).
11. W. Sun et al., "Zn/MnO_2 battery chemistry with H^+ and Zn^{2+} coinsertion." *J. Am. Chem. Soc.*, **139**, 9775 (2017).
12. J. Huang, Z. Wang, M. Hou, X. Dong, Y. Liu, Y. Wang, and Y. Xia, "Polyaniline-intercalated manganese dioxide nanolayers as a high-performance cathode material for an aqueous zinc-ion battery." *Nat. Commun.*, **9**, 2906 (2018).
13. D. Chao, W. Zhou, C. Ye, Q. Zhang, Y. Chen, L. Gu, K. Davey, and S.-Z. Qiao, "An electrolytic Zn-MnO_2 battery for high-voltage and scalable energy storage." *Angew. Chem., Int. Ed. Engl.*, **58**, 7823 (2019).
14. Y. Li, S. Wang, J. R. Salvador, J. Wu, B. Liu, W. Yang, J. Yang, W. Zhang, J. Liu, and J. Yang, "Reaction mechanisms for long-life rechargeable Zn/MnO_2 batteries." *Chem. Mater.*, **31**, 2036 (2019).
15. C. Guo, H. Liu, J. Li, Z. Hou, J. Liang, J. Zhou, Y. Zhu, and Y. Qian, "Ultrathin δ-MnO_2 nanosheets as cathode for aqueous rechargeable zinc ion battery." *Electrochim. Acta*, **304**, 370 (2019).
16. S. H. Kim and S. M. Oh, "Degradation mechanism of layered MnO_2 cathodes in Zn/$ZnSO_4$/MnO_2 rechargeable cells." *J. Power Sources*, **72**, 150 (1998).
17. A. S. Poyraz, J. Laughlin, and Z. Zec, "Improving the cycle life of cryptomelane type manganese dioxides in aqueous rechargeable zinc ion batteries: the effect of electrolyte concentration." *Electrochim. Acta*, **305**, 423 (2019).
18. I. Stosevski, A. Bonakdarpour, F. Cuadra, and D. P. Wilkinson, "Highly crystalline ramsdellite as a cathode material for near-neutral aqueous MnO_2/Zn batteries." *Chem. Commun.*, **55**, 2082 (2019).
19. J. Wang, J.-G. Wang, H. Liu, C. Wei, and F. Kang, "Zinc ion stabilized MnO_2 nanospheres for high capacity and long lifespan aqueous zinc-ion batteries." *J. Mater. Chem. A*, **16**, 16 (2019).
20. B. Wu, G. Zhang, M. Yan, T. Xiong, P. He, L. He, X. Xu, and L. Mai, "Graphene scroll-coated α-MnO_2 nanowires as high-performance cathode materials for aqueous Zn-ion battery." *Small*, **14**, e1703850 (2018).
21. C. Xu, H. Du, B. Li, F. Kang, and Y. Zeng, "Reversible insertion properties of zinc ion into manganese dioxide and its application for energy storage." *Electrochem. Solid-State Lett.*, **12**, A61 (2009).
22. S. Zhao, B. Han, D. Zhang, Q. Huang, L. Xiao, L. Chen, D. G. Ivey, Y. Deng, and W. Wei, "Unravelling the reaction chemistry and degradation mechanism in aqueous Zn/MnO_2 rechargeable batteries." *J. Mater. Chem. A*, **6**, 5733 (2018).
23. M. Chamoun, W. R. Brant, C.-W. Tai, G. Karlsson, and D. Noréus, "Rechargeability of aqueous sulfate Zn/MnO_2 batteries enhanced by accessible Mn^{2+} ions." *Energy Storage Mater.*, **15**, 351 (2018).
24. D. Wang, L. Wang, G. Liang, H. Li, Z. Liu, Z. Tang, J. Liang, and C. Zhi, "A superior δ-MnO_2 cathode and a self-healing Zn-δ-MnO_2 battery." *ACS Nano*, **13**, 10643 (2019).

25. G. Liang, F. Mo, H. Li, Z. Tang, Z. Liu, D. Wang, Q. Yang, L. Ma, and C. Zhi, "A universal principle to design reversible aqueous batteries based on deposition–dissolution mechanism." *Adv. Energy Mater.*, **9**, 1901838 (2019).
26. L. Wang et al., "Silver-containing α-MnO_2 nanorods: electrochemistry in rechargeable aqueous Zn-MnO_2 batteries." *J. Electrochem. Soc.*, **166**, A3575 (2019).
27. H. Li, C. Xu, C. Han, Y. Chen, C. Wei, B. Li, and F. Kang, "Enhancement on cycle performance of Zn anodes by activated carbon modification for neutral rechargeable zinc ion batteries." *J. Electrochem. Soc.*, **162**, A1439 (2015).
28. H. Li et al., "An extremely safe and wearable solid-state zinc ion battery based on a hierarchical structured polymer electrolyte." *Energy Environ. Sci.*, **11**, 941 (2018).
29. W. Qiu, Y. Li, A. You, Z. Zhang, G. Li, X. Lu, and Y. Tong, "High-performance flexible quasi-solid-state Zn–MnO_2 battery based on MnO_2 nanorod arrays coated 3D porous nitrogen-doped carbon cloth." *J. Mater. Chem. A*, **5**, 14838 (2017).
30. W. Kao-ian, R. Pornprasertsuk, P. Thamyongkit, T. Maiyalagan, and S. Kheawhom, "Rechargeable zinc-ion battery based on choline chloride-urea deep eutectic solvent." *J. Electrochem. Soc.*, **166**, A1063 (2019).
31. C. E. Mortimer, U. Müller, and J. Beck, in *Chemie. Das Basiswissen der Chemie* (Thieme , Stuttgart) (2015) 978-3-13-484312-512.
32. P. Atkins and J. D. Paula, in *Physical Chemistry* (W. H. Freeman and Company, New York) 9th ed., ISBN 9781429218122 (2010).
33. A. Bard, in *Standard Potentials in Aqueous Solution* (Taylor and Francis, London) 1st ed., ISBN 9781351414746 (2017).
34. J. Stamm, A. Varzi, A. Latz, and B. Horstmann, "Modeling nucleation and growth of zinc oxide during discharge of primary zinc-air batteries." *J. Power Sources*, **360**, 136 (2017).
35. F. Sagane, K.-I. Ikeda, K. Okita, H. Sano, H. Sakaebe, and Y. Iriyama, "Effects of current densities on the lithium plating morphology at a lithium phosphorus oxynitride glass electrolyte/copper thin film interface." *J. Power Sources*, **233**, 34 (2013).
36. Z. Hou, X. Zhang, X. Li, Y. Zhu, J. Liang, and Y. Qian, "Surfactant widens the electrochemical window of an aqueous electrolyte for better rechargeable aqueous sodium/zinc battery." *J. Mater. Chem. A*, **5**, 730 (2017).
37. M. H. Alfaruqi, J. Gim, S. Kim, J. Song, D. T. Pham, J. Jo, Z. Xiu, V. Mathew, and J. Kim, "A layered δ-MnO_2 nanoflake cathode with high zinc-storage capacities for eco-friendly battery applications." *Electrochem. Commun.*, **60**, 121 (2015).
38. M. H. Alfaruqi, S. Islam, D. Y. Putro, V. Mathew, S. Kim, J. Jo, S. Kim, Y.-K. Sun, K. Kim, and J. Kim, "Structural transformation and electrochemical study of layered MnO_2 in rechargeable aqueous zinc-ion battery." *Electrochim. Acta*, **276**, 1 (2018).
39. X. Guo, J. Li, X. Jin, Y. Han, Y. Lin, Z. Lei, S. Wang, L. Qin, S. Jiao, and R. Cao, "A hollow-structured manganese oxide cathode for stable Zn-MnO_2 batteries." *Nanomaterials*, **8**, 301 (2018).
40. S. Islam et al., "Facile synthesis and the exploration of the zinc storage mechanism of β-MnO_2 nanorods with exposed (101) planes as a novel cathode material for high performance eco-friendly zinc-ion batteries." *J. Mater. Chem. A*, **5**, 23299 (2017).
41. T. Shoji, M. Hishinuma, and T. Yamamoto, "Zinc-manganese dioxide galvanic cell using zinc sulphate as electrolyte. Rechargeability of the cell." *J. Appl. Electrochem.*, **18**, 521 (1988).
42. X. Wang, S. Zheng, F. Zhou, J. Qin, X. Shi, S. Wang, C. Sun, X. Bao, and Z.-S. Wu, "Scalable fabrication of printed Zn//MnO_2 planar micro-batteries with high volumetric energy density and exceptional safety." *Natl Sci. Rev.*, **6**, 1 (2019).
43. B. Lee, H. R. Lee, H. Kim, K. Y. Chung, B. W. Cho, and S. H. Oh, "Elucidating the intercalation mechanism of zinc ions into α-MnO_2 for rechargeable zinc batteries." *Chem. Commun. (Camb.)*, **51**, 9265 (2015).
44. J. Hao, J. Mou, J. Zhang, L. Dong, W. Liu, C. Xu, and F. Kang, "Electrochemically induced spinel-layered phase transition of Mn_3O_4 in high performance neutral aqueous rechargeable zinc battery." *Electrochim. Acta*, **259**, 170 (2018).
45. S. Yang, M. Zhang, X. Wu, X. Wu, F. Zeng, Y. Li, S. Duan, D. Fan, Y. Yang, and X. Wu, "The excellent electrochemical performances of $ZnMn_2O_4$/Mn_2O_3: the composite cathode material for potential aqueous zinc ion batteries." *J. Electroanal. Chem.*, **832**, 69 (2019).
46. N. Zhang, F. Cheng, Y. Liu, Q. Zhao, K. Lei, C. Chen, X. Liu, and J. Chen, "Cation-deficient spinel $ZnMn_2O_4$ cathode in $Zn(CF_3SO_3)_2$ electrolyte for rechargeable aqueous Zn-ion battery." *J. Am. Chem. Soc.*, **138**, 12894 (2016).
47. B. Jiang, C. Xu, C. Wu, L. Dong, J. Li, and F. Kang, "Manganese sesquioxide as cathode material for multivalent zinc ion battery with high capacity and long cycle life." *Electrochim. Acta*, **229**, 422 (2017).
48. D. Xu, B. Li, C. Wei, Y.-B. He, H. Du, X. Chu, X. Qin, Q.-H. Yang, and F. Kang, "Preparation and characterization of MnO_2/acid-treated CNT nanocomposites for energy storage with zinc ions." *Electrochim. Acta*, **133**, 254 (2014).
49. Y. Huang, J. Mou, W. Liu, X. Wang, L. Dong, F. Kang, and C. Xu, "Novel insights into energy storage mechanism of aqueous rechargeable Zn/MnO_2 batteries with participation of Mn^{2+}." *Nano-Micro Lett.*, **11**, 860 (2019).
50. A. Jain et al., "Commentary: the materials project: a materials genome approach to accelerating materials innovation." *APL Mater.*, **1**, 11002 (2013).